Supplement of Nat. Hazards Earth Syst. Sci., 19, 2811–2825, 2019
https://doi.org/10.5194/nhess-19-2811-2019-supplement

Natural Hazards and Earth System Sciences
Open Access

Supplement of

Infrasound and seismoacoustic signatures of the 28 September 2018 Sulawesi super-shear earthquake

Christoph Pilger et al.

Correspondence to: Christoph Pilger (christoph.pilger@bgr.de)

Supplementary Material

Figure S1

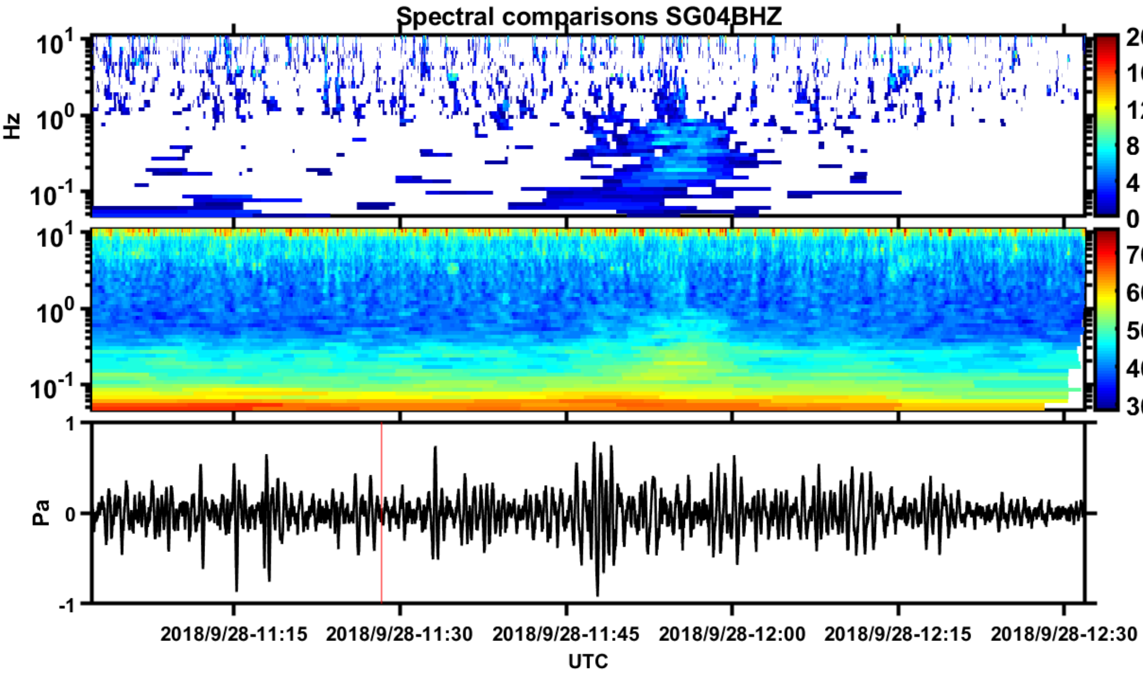

Fig S1: Example of INFERNO analysis for the Singapore station (SING). The bottom panel is the waveform recorded at sensor SG04, with the red vertical line representing an estimated arrival time based on the location and time of the earthquake. The middle panel is an example of an INFERNO spectrogram where energy is calculated in fractional octave bands. The top panel is a signal to noise plot derived from the spectrogram. All the values for each frequency band are averaged and a 3dB threshold is set. Note that while the signal from the event is not as obvious within the waveform and spectrogram, the signal to noise plot clearly shows the signals arrival.

Figure S2

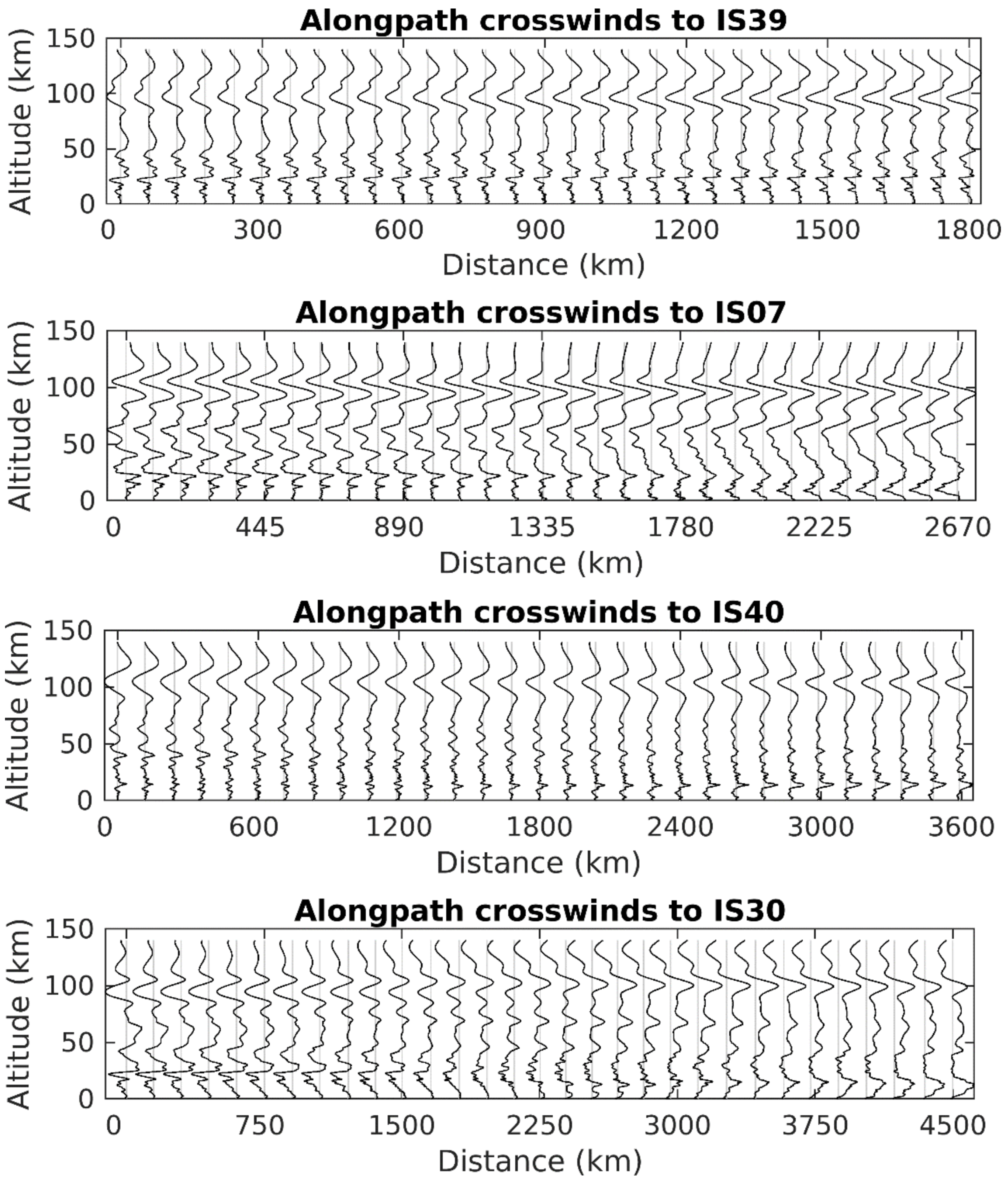

Fig S2: Crosswind profiles along the propagation path from the epicenter to the four arrays. Positive values correspond to winds in the 90° clockwise perpendicular direction, the distance between two vertical lines corresponds to 50 m/s wind intensity. Range-dependent ECMWF profiles merged with climatologies are used as described in the data section. Enhanced positive crosswinds potentially responsible for positive back-azimuth deviations occur at I39PW around the stratospheric turning altitude of 50 km and to some degree below that altitude. Strong negative crosswinds at 50 km altitude and below occur at I07AU and might explain negative back-azimuth deviations for this station. Weak total crosswinds at and below 50 km at station I40PG might explain marginal back-azimuth deviations at this station. Strong thermospheric crosswinds around 100 km and below might explain back-azimuth deviations at I30JP after thermospheric propagation.

Figure S3

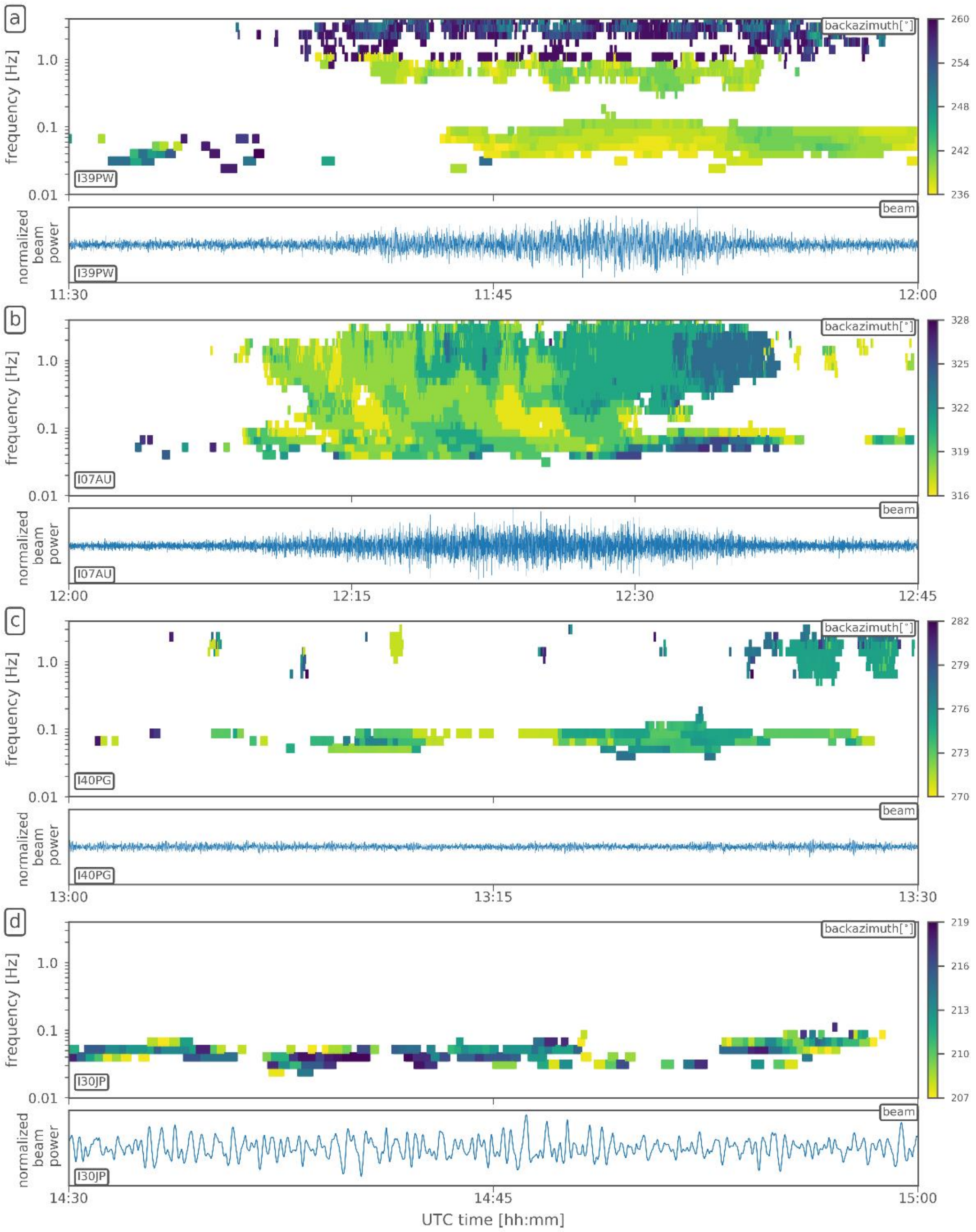

Fig S3: Waveform beams and PMCC backazimuth information for the four infrasound arrays of figure 2. Absolute backazimuth directions are provided here instead of epicentral deviations, allowing to quantify changes and differences in the direction of signal origin. A small azimuthal section (±12° from the expected epicenter direction in subfigure a, ±6° in subfigure b, c and d) and short time window (30 min in subfigures a, c and d, 45 min in subfigure b) is chosen to highlight the epicentral infrasound's origin direction and arrival time as specified in table 1. Differences in the direction of origin between the high-frequency and the mid- to low-frequency parts of the epicentral infrasound are found at I39PW (subfigure a) in the order of ±10°. An azimuthal sweep of about 7° is observed at I07AU (subfigure b). Both phenomena indicate a spatially and temporally extended source. Only small and mostly arbitrary backazimuth variation is present at stations I40PG and I30JP (subfigures c and d).

Figure S4

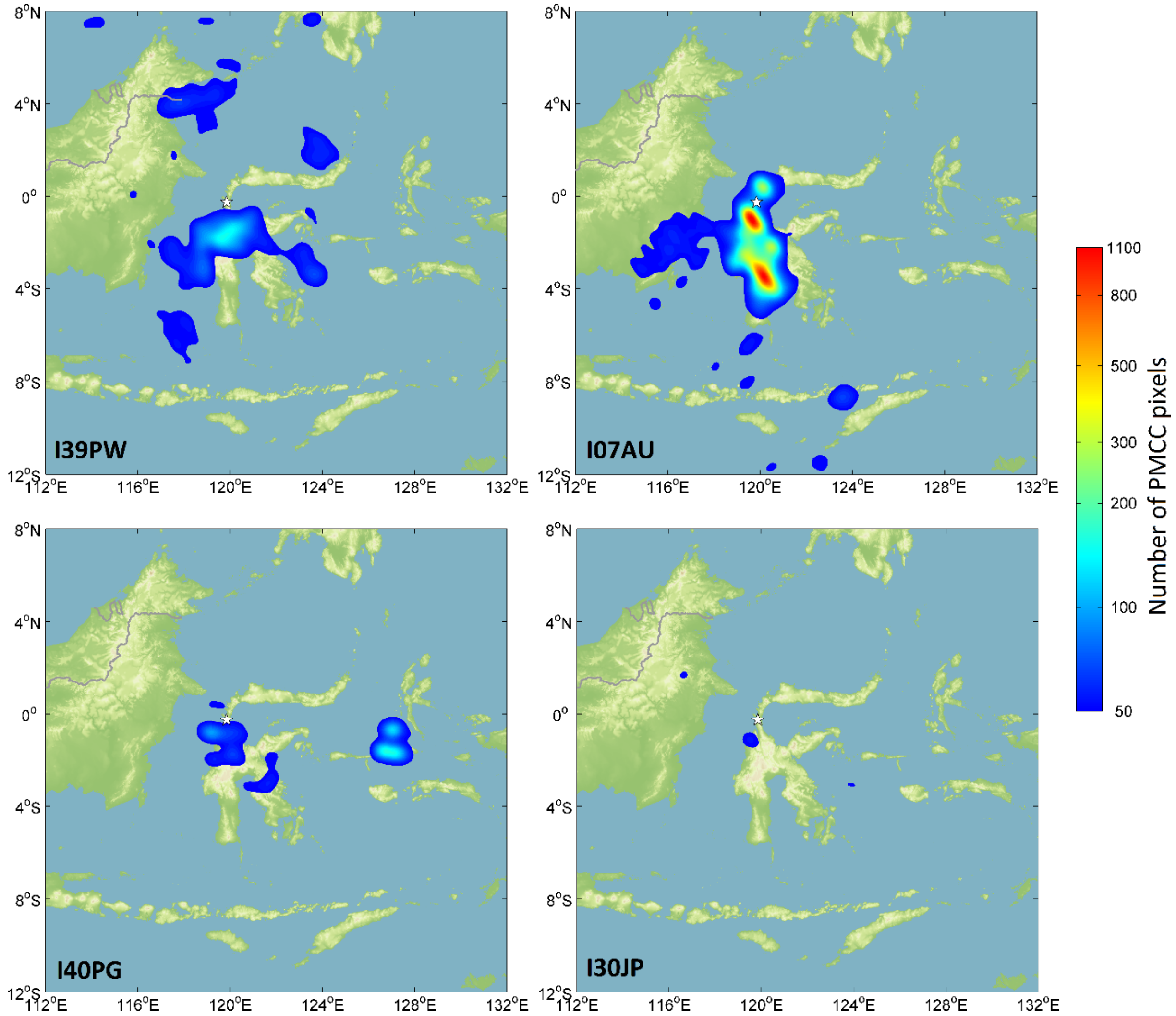

Fig S4: Single-station back projection maps for the four infrasound arrays. The colorbar of each figure starts at a 4 time lower value than in the cumulative 4-station-figure 5. The main region near the epicenter (marked by a star) and the rupture south of it are projected reasonably well for each station. The directional deviation and spatial extension of the back-projected source regions per station corresponds to backazimuth variations as e.g. the azimuthal sweep in figure S3. Additionally, regions of potential seismoacoustic signal generation are identified around the island of Sulawesi, as described in the manuscript text.